Journal of Power Sources 196 (2011) 6934–6938

Contents lists available at ScienceDirect

Journal of Power Sources

journal homepage: www.elsevier.com/locate/jpowsour

Short communication

Synthesis, phase relation and electrical and electrochemical properties of ruthenium-substituted Li_2MnO_3 as a novel cathode material

Daisuke Mori[a,*], Hikari Sakaebe[b], Masahiro Shikano[b], Hiroshi Kojitani[a], Kuniaki Tatsumi[b], Yoshiyuki Inaguma[a]

[a] Department of Chemistry, Faculty of Science, Gakushuin University, 1-5-1 Mejiro, Toshima-ku, Tokyo 171-8588, Japan
[b] Research Institute for Ubiquitous Energy Devices, National Institute of Advanced Industrial Science and Technology (AIST), 1-8-31 Midorigaoka, Ikeda, Osaka 563-8577, Japan

ARTICLE INFO

Article history:
Received 7 September 2010
Received in revised form 28 October 2010
Accepted 29 November 2010
Available online 4 December 2010

Keywords:
Lithium manganese oxide
Ruthenium substitution
Cathode material
Lithium battery

ABSTRACT

Layered oxides, ruthenium-substituted Li_2MnO_3, were synthesized at 800 °C and 1200 °C. Their phase relation and electrical and electrochemical properties were investigated. $Li_2Mn_{1-x}Ru_xO_3$ synthesized at 800 °C clearly separated into two phases, manganese-rich and ruthenium-rich phases, except for the narrow composition range of $0 \le x \le 0.05$, while $Li_2Mn_{1-x}Ru_xO_3$ synthesized at 1200 °C formed two solid solutions in the whole composition range across a structural transition between $x = 0.6$ and 0.8. The electrical resistivity of $Li_2Mn_{1-x}Ru_xO_3$ decreased with increasing ruthenium content. $Li_2Mn_{0.2}Ru_{0.8}O_3$ ($x = 0.8$) synthesized at 1200 °C showed the lowest resistivity of $5.7 \times 10^2\ \Omega$ cm at room temperature. The discharge capacity and cycling performance were improved by the ruthenium substitution. $Li_2Mn_{0.4}Ru_{0.6}O_3$ ($x = 0.6$) exhibited a discharge capacity of 192 mAh g^{-1} in the initial cycle and 169 mAh g^{-1} in the tenth cycle with high and almost constant charge–discharge efficiencies of 99% from the second to tenth cycle at a current rate of 1/10*C*. The ruthenium substitution to Li_2MnO_3 is quite effective to improve electrical conductivity and charge–discharge performance.

© 2010 Elsevier B.V. All rights reserved.

1. Introduction

Much attention has been paid to lithium batteries as an indispensable energy storage system for portable electric devices, electric power tools, hybrid electric vehicles (HEV) and pure electric vehicles (EV). Lithium manganese oxide (Li_2MnO_3) is a promising candidate as an alternative cathode material having higher voltage, larger theoretical capacity of about 460 mAh g^{-1}. In case all lithium ions are utilized, lower cost and lower environmental impact. Li_2MnO_3 has similar layered structure to the practical cathode materials represented as $LiMO_2$ (M = transition metal) with layered rocksalt-type structure. The schematic drawing of Li_2MnO_3 structure is shown in Fig. 1. It consists of lithium layer and lithium–manganese mixed layer situated alternately between closed packing oxygen layers.

Chemical leached Li_2MnO_3 showing the capacity of approximately 200 mAh g^{-1} was studied by Rossouw and Thackeray [1]. Li_2MnO_3 synthesized at low temperature also exhibited high specific capacity of 160–260 mAh g^{-1} [2–4]. Iron-substituted Li_2MnO_3 synthesized by hydrothermal method was proposed as a high capacity cathode material [5,6]. Li_2MnO_3 was generally considered electrochemical inactive because tetravalent manganese ion is hardly oxidized in an octahedral coordination. Therefore, several mechanistic studies were performed to explain the electrochemical activity of Li_2MnO_3 [2,3,7–10]. It was suggested that lithium removal accompanied with charge compensation by the oxidation of oxygen occurs at about 4.6 V [7]. Li_2O removal and oxygen loss were proposed as the origin of electrochemical activity of Li_2MnO_3 [1–3,10,11]. On the other hand, it was attributed to ion-exchange of lithium by proton generated by oxidation of the nonaqueous electrolyte [2]. The mechanism of electrochemical reaction of Li_2MnO_3 remains controversial. Meanwhile, there are several problems in practical use of Li_2MnO_3 as the cathode material. To emerge electrochemical activity of Li_2MnO_3, reducing particle size and oxygen removal are necessary due to its low ionic and electronic conductivities. Li_2MnO_3 also showed poor cycling performance, which is attributed to the structural transition from layered structure to spinel-like structure [2,3,12].

The electrochemical properties of other Li_2MO_3-type oxides (M = Mo, Ru, Ir, and Pt) containing 4d and 5d transition metals with the similar layered structure to Li_2MnO_3 were also investigated [13–18]. The electrochemical measurements of Li/Li_2MO_3 (M = Mo, Ru, Ir, and Pt) cells confirmed that $Mo^{5+/4+}$, $Ru^{5+/4+}$, $Ir^{5+/4+}$ and $Pt^{5+/4+}$ couples permit lithium extraction from the host structure. In particular, Li_2RuO_3 showed relatively high specific capacity of 160 mAh g^{-1} with a voltage range of 3.0–4.0 V and good reversibil-

* Corresponding author. Tel.: +81 3 3986 0221; fax: +81 3 5992 1029.
E-mail address: daisuke.mori@gakushuin.ac.jp (D. Mori).

0378-7753/$ – see front matter © 2010 Elsevier B.V. All rights reserved.
doi:10.1016/j.jpowsour.2010.11.150

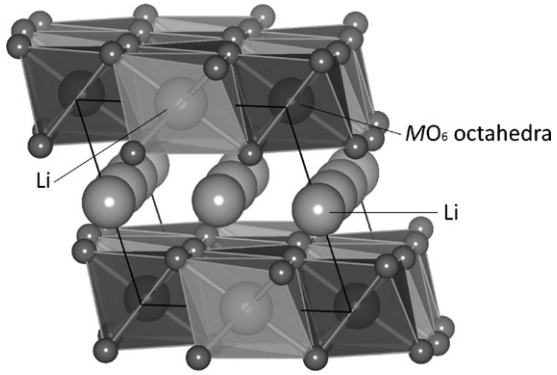

Fig. 1. Schematic drawing of Li_2MnO_3 structure.

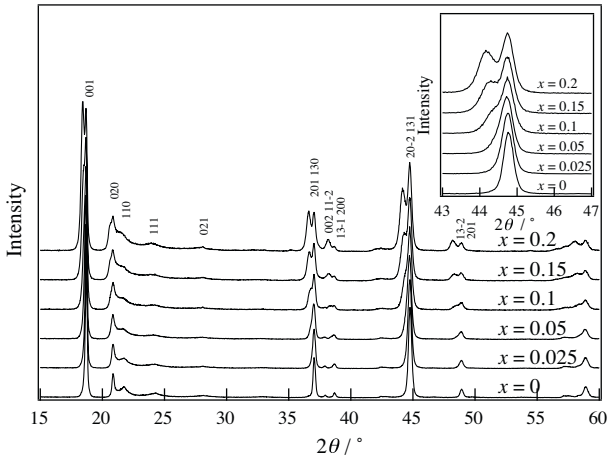

Fig. 2. XRD patterns for $Li_2Mn_{1-x}Ru_xO_3$ synthesized at 800 °C. The inset shows magnified XRD patterns around $2\theta = 45°$.

ity because of the tightly composed host lattice [13]. In addition, Li_2RuO_3 exhibited significant lower resistivity of 10 Ω cm than that of Li_2MnO_3 at room temperature [14,19]. Li_2RuO_3 has complementary properties to those of Li_2MnO_3. However, the electrical and electrochemical properties of the solid solution between Li_2MnO_3 and Li_2RuO_3 have not been studied. There is single literature in our knowledge that magnetic property of ruthenium-substituted Li_2MnO_3 was investigated [20]. Therefore, in the present study we synthesized the ruthenium-substituted Li_2MnO_3 as a novel cathode material to improve the cycling performance by stabilizing the host structure during the lithium (de-)intercalation and the electrochemical activity due to a decrease in electrical resistivity. The relationship between synthesis condition, phase relation and electrical and electrochemical properties is discussed.

2. Experimental

The ruthenium-substituted lithium manganese oxide, $Li_2Mn_{1-x}Ru_xO_3$, was synthesized at 800 °C and 1200 °C. Li_2CO_3 (Kojundo Chemical Laboratory Co., Ltd., 99.99%), MnO_2 (Rare Metallic Co., Ltd., 99.9%) and RuO_2 (Rare Metallic Co., Ltd., 99.9%) were weighed, mixed and pelletized. $Li_2Mn_{1-x}Ru_xO_3$ in the range of $0 \le x \le 0.2$ was synthesized at 800 °C with a following procedure. The pelletized sample was calcined at 600 °C for 12 h. After grinding, the calcined powder was again pelletized and sintered at 800 °C for 24 h in an oxygen gas flow. On the other hand, $Li_2Mn_{1-x}Ru_xO_3$ in the range of $0 < x < 1.0$ was synthesized by firing at 1200 °C for 3 h twice with an intermediate grinding in an oxygen gas flow. The $Li_2Mn_{1-x}Ru_xO_3$ synthesized at 800 and 1200 °C are hereafter referred to as LMR-800 and LMR-1200, respectively. The both end members, Li_2MnO_3 and Li_2RuO_3, were synthesized by firing at 600 °C and then at 1000 °C for 3 h twice with intermediate grindings in an oxygen gas flow.

The powdered samples obtained were identified by the X-ray diffraction (XRD) measurement with Rigaku RINT 2100 diffractometer using monochromatic Cu Kα line. The polished sample was characterized by a scanning electron microscope (SEM) (JSM-6360, JEOL) with an energy dispersive X-ray spectrometer (EDS) (INCA Energy 300, Oxford Instruments). The acceleration voltage of an electron beam was 15 kV. The sample composition was then determined by taking an average of the values at ten points measured using EDS. The electrical resistivity was measured by the dc four-prove method with a silver paste contact for the LMR-800 in the range of $0.1 \le x \le 0.2$ and LMR-1200. The electrical resistivity measurements were performed for the LMR-800 in the range of $0 \le x < 0.1$ by the ac impedance measurement using a precision LCR meter (4284A, Agilent Technology) with a frequency range between about 100 and 1 MHz. The extrapolated low-frequency intercept of the semi-circle with the real axis was regarded as the sample resistivity. The crystal structure was drawn using the program VESTA [21].

The electrochemical properties were investigated using flat-type HS cell (Hohsen Corp.). The positive electrode comprised the sample, acetylene black (HS-100, DENKA) and poly(vinylidene difluoride) (PVdF) binder (KF1320, Kureha Corp.) with a weight ratio of 10:1.5:1.5 coated onto aluminum current collector. 1 M $LiPF_6$ in EC/DMC with a volume ratio of 1:2 and lithium metal were used as the electrolyte and the negative electrode, respectively. The charge–discharge property was examined at 25 °C with a voltage range between 2.0 and 4.8 V vs. Li/Li^+ with a constant current rate of 1/10C. Here the current rate was calculated from the theoretical capacity in case lithium in lithium layer is utilized.

3. Results and discussion

The XRD patterns for the LMR-800 in the range of $0 \le x \le 0.2$ are shown in Fig. 2. All of the reflections of Li_2MnO_3 ($x = 0$) were indexed in the monoclinic lattice with the space group $C2/m$ [22,23]. The broad peaks around 20–25° in the pattern for Li_2MnO_3 are similar to those reported previously [24], which is attributed to the ordering of lithium and manganese in the transition metal layer. The peak broadening is caused by an increase of the degree of stacking fault [25]. The reflections of LMR-800 shifted to low-angle side with increasing ruthenium content at the range of $x \le 0.05$, which indicates that the LMR-800 formed a solid solution. Additional reflections appeared at lower-angle side of the parent reflection and the parent reflections slightly shifted to the opposite side for the LMR-800 with $x = 0.1$. In the range of $0.1 \le x \le 0.2$ the parent reflections did not shift, while the additional reflections shifted to low-angle side and their intensity increased with increasing ruthenium content. Therefore, these results indicate that a phase separation into manganese-rich and ruthenium-rich phases occurs in the LMR-800 at the range of $0.1 \le x \le 0.2$. The XRD measurement indicated that the formation of the manganese-rich phase proceeded during the calcination at 600 °C and RuO_2 used as a stating material remained. Once manganese-rich phase formed, the formation of solid solution does not proceed during sintering at 800–1200 °C. It is found that high calcining temperature is required to obtain a single phase of $Li_2Mn_{1-x}Ru_xO_3$.

Fig. 3 shows the XRD patterns for the LMR-1200 with the range of $0 < x < 1.0$ and both end members ($x = 0$, 1.0) synthesized at 1000 °C. The XRD patterns for the both end members are quite similar to those in the literature [13,25]. The reflections showed a continuous shift from Li_2MnO_3 to Li_2RuO_3 in the diffraction

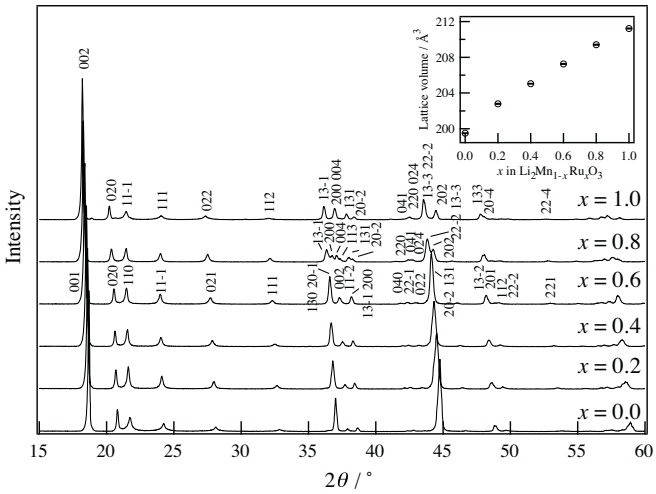

Fig. 3. XRD patterns for $Li_2Mn_{1-x}Ru_xO_3$ synthesized at 1200 °C. The inset shows compositon dependence of lattice volume of the LMR-1200.

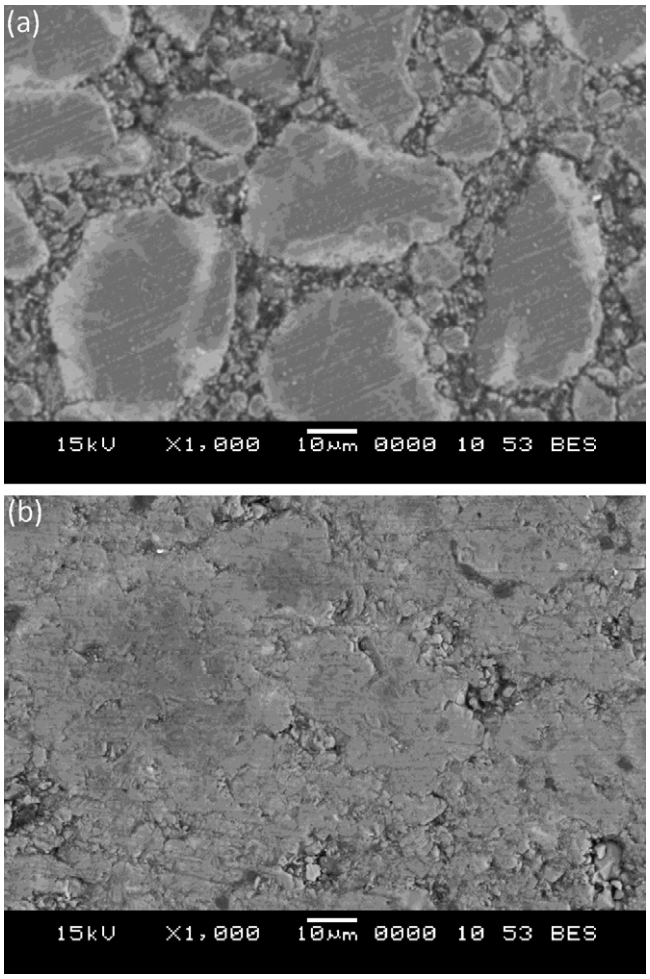

Fig. 4. SEM photograph of $Li_2Mn_{0.8}Ru_{0.2}O_3$ (x = 0.2) synthesized at 800 °C (a) and 1200 °C (b).

patterns for $Li_2Mn_{1-x}Ru_xO_3$, which suggests single-phase samples were obtained in the whole composition range. The $Li_2Mn_{1-x}Ru_xO_3$ system has two solid solutions in composition regions, $0 \le x \le 0.6$ and $0.8 \le x \le 1.0$. The former adopts Li_2MnO_3-type structure and the latter adopts the Li_2RuO_3-type structure. The Li_2MO_3 type oxides have different stackings of cation layers along *c*-axis. The Li_2MnO_3 have successive $[Li_{1/3}Mn_{2/3}]$ layers displaced by the (0, 0, 1) translation, which leads to the stacking sequence with the mirror plane perpendicular to *b*-axis [25]. While, Li_2RuO_3 has the similar $[Li_{1/3}Ru_{2/3}]$ layers displaced by the (0, 1/2, 1/2) translation, which leads to the stacking sequence with the *c*-glide plane perpendicular to *b*-axis [13]. The composition dependence of lattice volume of LMR-1200 is shown in an inset of Fig. 3. The lattice volume varied monotonously into Li_2RuO_3 containing tetravalent ruthenium as ruthenium content increases. It indicates that the LMR-1200 shows no significant change in the valence state of ruthenium by the substitution. Therefore, ruthenium is considered to be tetravalent in the LMR-1200 system.

The SEM photographs for the LMR-800 and LMR-1200 at $x = 0.2$ are shown in Fig. 4. It was confirmed that the LMR-800 clearly separated into two phases. The sample formed aggregates consisting of inner dark phase and outer bright phase. EDS analysis of the LMR-800 revealed that average molar ratios of manganese and ruthenium in the inner dark phase and outer bright phase were 99.24(18):0.76(19) and 32(3):68(3), respectively. The figures in parentheses represent twice standard deviation of the mean. It is consistent with the XRD results that the LMR-800 has manganese-rich and ruthenium-rich phases. On the other hand, the LMR-1200 did not clearly exhibit phase separation. The LMR-1200 had an average molar ratio of manganese and ruthenium of 83.6(13):16.4(13). The composition of LMR-1200 showed a slight deviation from the nominal composition due to the volatilization of ruthenium with a certain level of compositional fluctuation. Compositional fluctuation is observed for the iron-substituted lithium manganese oxide which has nano-domain structure consisting of iron and manganese domains [10]. The nano-domain structure provides electrochemical activity to both α-$LiFeO_2$ and Li_2MnO_3 which are electrochemical inactive as pure bulk.

The electrical resistivity measurements were performed for LMR-800 and LMR-1200. The temperature dependence of electrical resistivity for the $Li_2Mn_{1-x}Ru_xO_3$ is shown in Fig. 5. All the samples exhibited semiconducting behavior. However, they did not obey the simple Arrhenius-type semiconducting model. No significant change in resistivity was observed for all samples in the range of temperature studied. The electrical resistivity of both the LMR-800 and LMR-1200 decreased with increasing ruthenium content. The resistivity of Li_2MnO_3 ($x = 0$) at room temperature was consistent with the literature one [19]. The LMR-800 with $x = 0.05$ showed lower electrical resistivity by two orders of magnitude than Li_2MnO_3. The resistivity of LMR-1200 in the range of $0.2 \le x \le 0.8$ was 10^2–10^3 Ω cm order at room temperature. The LMR-1200 with $x = 0.8$ showed the lowest resistivity of 5.7×10^2 Ω cm at room temperature. The oxides containing ruthenium of 4d transition metal mainly show metallic property because of its wide bandwidth [26–28]. The ruthenium substitution would induce to increase the overlap integral composed of transition metal t_{2g} orbitals and oxygen 2p orbitals in edge-shared MO_6 octahedra. The ruthenium substitution is quite effective to enhance the electrical conductivity of Li_2MnO_3.

Charge and discharge measurements on cells containing $Li_2Mn_{1-x}Ru_xO_3$ as the active cathode material were carried out in the voltage range of 2.0–4.8 V. Fig. 6 shows the charge and discharge profiles of initial cycle for the LMR-800 and LMR-1200. The charge profiles of the both $Li_2Mn_{1-x}Ru_xO_3$ samples were different from that of Li_2MnO_3 in which the cell voltage increases rapidly at the start of charge process and then a plateau appears around 4.5 V [2,3]. The charge and discharge profiles of the both $Li_2Mn_{1-x}Ru_xO_3$ samples were also different from that of Li_2RuO_3 [13]. Two distinct plateaus indicative of the multiphasic reactions were observed around 3.4 V and 3.6 V in the charge and discharge profiles of Li_2RuO_3.

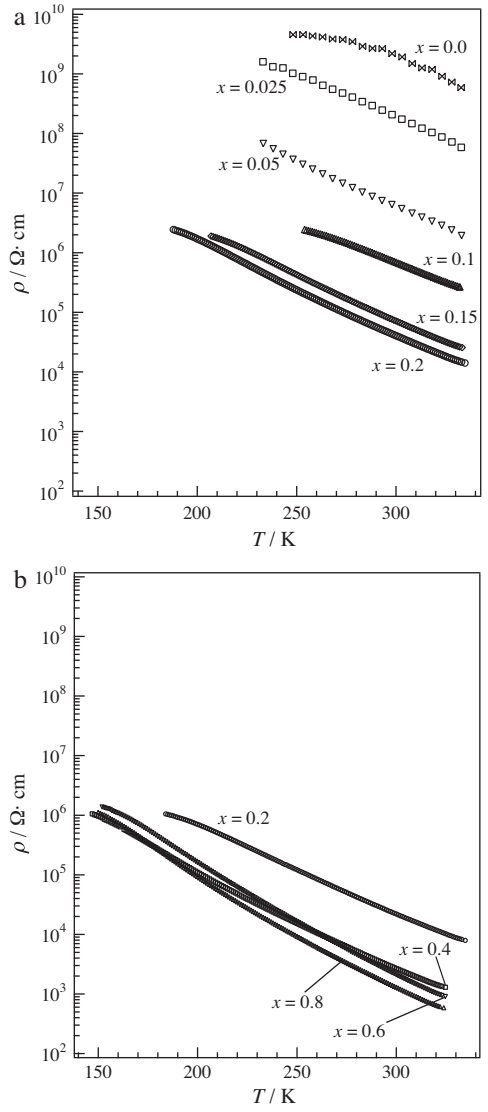

Fig. 5. Temperature dependence of elecrical resistivity for $Li_2Mn_{1-x}Ru_xO_3$ synthesized at 800 °C (a) and 1200 °C (b).

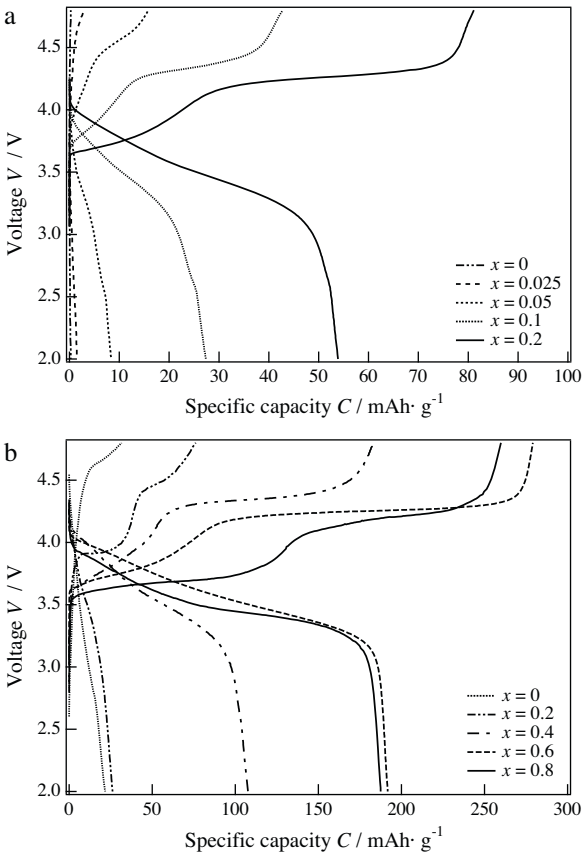

Fig. 6. Charge and discharge profiles of $Li_2Mn_{1-x}Ru_xO_3$ synthesized at 800 °C (a) and 1200 °C (b) in the voltage range of 2.0–4.8 V at 1/10 C rate.

The initial charge and discharge capacities of LMR-800 increased monotonously with increasing ruthenium content. The slope of charge profile of the LMR-800 in the range of $0 < x \leq 0.2$ changed around 4.2–4.5 V, which indicates that there are two processes in the initial charge reaction. The charge capacity corresponding to the both processes increased with increasing ruthenium content. This means that the substituted ruthenium ions were involved in the both processes. Therefore, the increase of capacity for LMR-800 is attributed to an increase of the amount of electrochemical active ruthenium-rich phase by ruthenium substitution. The charge voltage of the latter process lowered with increasing ruthenium content. It would be caused by a decrease in polarization due to the enhancement of electrical conductivity of $Li_2Mn_{1-x}Ru_xO_3$ depending on the ruthenium content.

The LMR-1200 in the range of $0.2 \leq x \leq 0.8$ also had two processes in the charge reaction. The charge capacities corresponding to the both processes increased with increasing ruthenium content up to $x = 0.6$. For the LMR-1200 at $x = 0.8$ the charge capacity corresponding to the former process increased more than expected, while the capacity corresponding to the latter process showed a sudden decrease. The discharge capacities also increased with increasing the ruthenium content in the range of $0 \leq x \leq 0.6$. However, the discharge capacity of the sample at $x = 0.8$ compared with that of the sample at $x = 0.6$. The irreversible capacity of the sample at $x = 0.8$ is lower than that at $x = 0.6$. The shape and voltage of the slope in the charge and discharge profile of the sample at $x = 0.8$ were clearly different from those of the samples in the range of $0 \leq x \leq 0.6$. They suggested that the charge and discharge mechanism of LMR-1200 changed accompanied with the structural transition from Li_2MnO_3-type to the Li_2RuO_3-type structure between $x = 0.6$ and 0.8 (see Fig. 3).

The cycle dependence of charge–discharge capacity and efficiency for the cells containing LMR-1200 at $x = 0.6$ and $x = 0.8$ are shown in Fig. 7. The cell containing the LMR-1200 at $x = 0.6$ exhibited a discharge capacity of 192 mAh g^{-1} in the first cycle and a reversible capacity of 183 mAh g^{-1} in a subsequent cycle. The discharge capacity in the tenth cycle reached 169 mAh g^{-1}, which indicates a relatively good cyclic retention. The cell containing the LMR-1200 at $x = 0.8$ also exhibited good cyclic retention as well as the sample at $x = 0.6$. Both cells also showed a good cyclic performance in terms of charge–discharge efficiency. In particular, the cell containing the LMR-1200 at $x = 0.6$ showed high and almost constant charge–discharge efficiencies of 99% from the second to tenth cycle. These results demonstrate that the ruthenium substitution to Li_2MnO_3 is quite fruitful to improve charge–discharge property. The $[(1/3)Li(2/3)RuO_3]_\infty$ hosts formed by the ruthenium substitution would improve structural stability and allows smooth lithium deintercalation/intercalation. It provides the superior specific capacity and cyclic performance of $Li_2Mn_{1-x}Ru_xO_3$. It is reported that the high reversibility of the Li/Li_2RuO_3 cell is related to the tightly composed $[(1/3)Li(2/3)RuO_3]_\infty$ hosts [13]. The ruthenium substitution significantly lowered electrical resistivity, which would lead to the enhancement of rate capability.

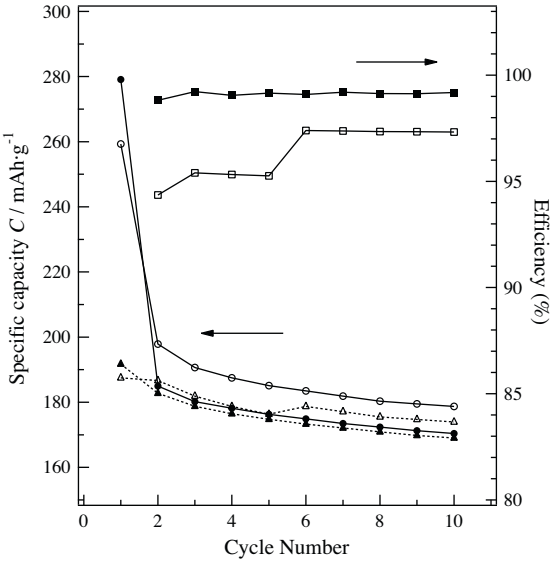

Fig. 7. Cycle dependence of charge and discharge capacities and efficiency of $Li_2Mn_{1-x}Ru_xO_3$ at $x = 0.6$ and 0.8. ●, ▲, and ■: Charge and discharge capacities and efficiency of $x = 0.6$, ○, △, and □: charge and discharge capacities and efficiency of $x = 0.8$.

To understand the detailed relationship between the ruthenium substitution and good cyclic performance, further structural study of $Li_2Mn_{1-x}Ru_xO_3$ during and after charge–discharge cycling is required. The electrochemical properties of $Li_2Mn_{1-x}Ru_xO_3$ were preliminarily investigated in this study and the optimization of the cell component such as control of particle size is expected to improve the electrochemical performance of $Li_2Mn_{1-x}Ru_xO_3$.

4. Conclusion

The tetravalent ruthenium-substituted Li_2MnO_3 as a novel cathode material was synthesized by solid-state reaction. The phase relation of $Li_2Mn_{1-x}Ru_xO_3$ depended on the synthesis condition. $Li_2Mn_{1-x}Ru_xO_3$ synthesized at 1200 °C formed two solid solutions in the whole composition range across a structural transition between $x = 0.6$ and 0.8. The electrical resistivity of ruthenium-substituted Li_2MnO_3 highly decreased with increasing ruthenium content, which would lead to the enhancement of rate capability. The ruthenium substitution to Li_2MnO_3 also improved the discharge capacity and cycling performance. It is attributed to increase electrochemical active ruthenium ion and the tightly composed $[(1/3)Li(2/3)RuO_3]$ hosts which allows smooth lithium deintercalation/intercalation. The ruthenium substitution is quite effective to bring out the potentially electrochemical performance of Li_2MnO_3.

References

[1] M.H. Rossouw, M.M. Thackeray, Mater. Res. Bull. 26 (1991) 463–473.
[2] A.D. Robertson, P.G. Bruce, Chem. Mater. 15 (2003) 1984–1992.
[3] D.Y.W. Yu, K. Yanagida, Y. Kato, H. Nakamura, J. Electrochem. Soc. 156 (2009) A417–A424.
[4] G.R. Jain, J.S. Yang, M. Balasubramanian, J.J. Xu, Chem. Mater. 17 (2005) 3850–3860.
[5] M. Tabuchi, Y. Nabeshima, K. Ado, M. Shikano, H. Kageyama, K. Tatsumi, J. Power Sources 174 (2007) 554–559.
[6] M. Tabuchi, A. Nakashima, H. Shigemura, K. Ado, H. Kobayashi, H. Sakaebe, H. Kageyama, T. Nakamura, M. Kohzaki, A. Hirano, R. Kanno, J. Electrochem. Soc. 149 (2002) A509–A524.
[7] Y. Koyama, I. Tanaka, M. Nagao, R. Kanno, J. Power Sources 189 (2009) 798–801.
[8] A.R. Armstrong, A.D. Robertson, P.G. Bruce, J. Power Sources 146 (2005) 275–280.
[9] D. Pasero, V. McLaren, S. de Souza, A.R. West, Chem. Mater. 17 (2005) 345–348.
[10] J. Kikkawa, T. Akita, M. Tabuchi, M. Shikano, K. Tatsumi, M. Kohyama, Electrochem. Solid-State Lett. 11 (2008) A183–A186.
[11] Z.H. Lu, J.R. Dahn, J. Electrochem. Soc. 149 (2002) A815–A822.
[12] C.S. Johnson, S.D. Korte, J.T. Vaughey, M.M. Thackeray, T.E. Bofinger, Y. Shao-Horn, S.A. Hackney, J. Power Sources 81 (1999) 491–495.
[13] H. Kobayashi, R. Kanno, Y. Kawamoto, M. Tabuchi, O. Nakamura, M. Takano, Solid State Ionics 82 (1995) 25–31.
[14] H. Kobayashi, R. Kanno, Y. Kawamoto, M. Tabuchi, O. Nakamura, Solid State Ionics 86–8 (1996) 859–863.
[15] H. Kobayashi, R. Kanno, M. Tabuchi, H. Kageyama, O. Nakamura, M. Takano, J. Power Sources 68 (1997) 686–691.
[16] H. Kobayashi, M. Tabuchi, M. Shikano, H. Kageyama, R. Kanno, J. Mater. Chem. 13 (2003) 957–962.
[17] H. Kobayashi, Y. Uebou, M. Tabuchi, H. Kageyama, Y. Yamamoto, M. Matsuoka, J. Tamaki, J. Electrochem. Soc. 150 (2003) A1408–A1415.
[18] K. Asakura, S. Okada, H. Arai, S. Tobishima, Y. Sakurai, J. Power Sources 81 (1999) 388–392.
[19] V. Massarotti, D. Capsoni, M. Bini, G. Chiodelli, C.B. Azzoni, M.C. Mozzati, A. Paleari, J. Solid State Chem. 131 (1997) 94–100.
[20] I. Felner, I.M. Bradaric, Physica B 311 (2002) 195–199.
[21] K. Momma, F. Izumi, J. Appl. Crystallogr. 41 (2008) 653–658.
[22] P. Strobel, B. Lambertandron, J. Solid State Chem. 75 (1988) 90–98.
[23] V. Massarotti, M. Bini, D. Capsoni, A. Altomare, A.G.G. Moliterni, J. Appl. Crystallogr. 30 (1997) 123–127.
[24] Y.S. Meng, G. Ceder, C.P. Grey, W.S. Yoon, M. Jiang, J. Bréger, Y. Shao-Horn, Chem. Mater. 17 (2005) 2386–2394.
[25] J. Bréger, M. Jiang, N. Dupré, Y.S. Meng, Y. Shao-Horn, G. Ceder, C.P. Grey, J. Solid State Chem. 178 (2005) 2575–2585.
[26] J.M. Longo, P.M. Raccah, J.B. Goodenough, Mater. Res. Bull. 4 (1969) 191–202.
[27] R.J. Bouchard, J.L. Gillson, Mater. Res. Bull. 6 (1971) 669–680.
[28] J.M. Longo, P.M. Raccah, J.B. Goodenough, J. Appl. Phys. 39 (1968) 1327–1328.